GEOLOGICA CARPATHICA, APRIL 2008, 59, 2, 117–132

Trace element chemistry of low-temperature pyrites — an indicator of past changes in fluid chemistry and fluid migration paths (Eger Graben, Czech Republic)

JIŘÍ ZACHARIÁŠ[1], JIŘÍ ADAMOVIČ[2] and ANNA LANGROVÁ[2]

[1]Institute of Geochemistry, Mineralogy and Mineral Resources, Faculty of Science, Charles University, Albertov 6, 128 43 Praha 2, Czech Republic; zachar@natur.cuni.cz
[2]Institute of Geology, Academy of Sciences CR, Rozvojová 269, 165 02 Praha 6, Czech Republic

(Manuscript received March 13, 2007; accepted in revised form November 13, 2007)

Abstract: Trace element contents in six generations of low-temperature (< ~50 °C) pyrite (Py-1 to Py-6) recognized in silicified Cretaceous sandstones near Jeníkov in the central Eger (Ohře) Graben, Bohemian Massif, are used to decipher late Cenozoic fluid circulation patterns in the graben. Py-1 and framboidal Py-2 are generally coeval with silica cementation, while Py-3 to Py-6 postdate this process. Py-6 forms inclusions in barite crystals, clearly separated in time from silica cementation. The average arsenic contents of 0.01, 0.15, 2.94, 3.91, 6.14 and 0.76 wt. % As for Py-1 through Py-6 and anomalous average nickel and cobalt contents in the oldest Py-6 inclusions (3.47 and 8.86 wt. %, respectively) indicate the presence of two contrasting fluid circulation patterns in the graben fill during the period of pyrite formation (?Pliocene to Recent). Early fluids (Py-1 to Py-5) are interpreted as progressive deepening, fault-driven fluids originating from acidic volcanics in the basement. The late fluids are shallow, topography-driven fluids in contact with the Tertiary lignite beds. Earlier data from structural geology allow us to explain such change in fluid circulation by regional tectonic stress rearrangement, which inhibited the activity on the Krušné hory Fault at about 400 ka.

Key words: Eger Graben, silicification, fluid chemistry, fluid circulation patterns, pyrite, arsenian pyrite, arsenic.

Introduction

Low-temperature formation of pyrite is associated with diagenetic processes in sediments, often combined with bacterial precipitation under anoxic conditions, and with hydrothermal activity at shallow depths under the surface. Pyrite is commonly a stoichiometric FeS_2 phase; however, significant amounts of As, Ni, Co and minor Au amounts were found in many natural samples. As-rich pyrites typically appear to have formed at relatively low temperatures and often exhibit habits that suggest rapid precipitation (Abraitis et al. 2004). The extent of As solubility and type of bonding in the pyrite structure (isomorphous $As_{+1}S_{-1}$ substitution vs. nanoinclusions of arsenopyrite) was recently discussed by Reich & Becker (2006). Klemm (1965) demonstrated experimentally extensive solid solutions between pyrite (FeS_2), cattierite (CoS_2), and vaesite (NiS_2) at high temperatures (~500 °C and higher), and limited ones at low temperatures. In contrast, low-temperature (< ~150 °C) pyrites are commonly rich in Co, or Ni, or both (bravoite). The formation temperatures of natural mineral assemblages are, however, still poorly constrained.

In the Eger (Ohře) Graben of the Bohemian Massif, low-temperature pyrite formation is associated with fluid advection along major faults in Cenozoic times. Flows of low-saline epithermal fluids were driven by topography, being heated on deep circulation paths, or by the heat gradient along subvolcanic bodies. These fluids were streamed into adjacent aquifers of coarse detrital sediments, thereby causing pervasive silicification and sulphidic mineralization in zones several kilometers broad. The lateral extent of the epithermal mineralization is further enhanced by the presence of sealing horizons above the aquifers.

In this paper we describe textural and chemical variations in six successive pyrite generations, all associated with low-temperature (~30–60 °C) shallow fossil subsurface geothermal discharge, in the silicified Lower Turonian quartzose sandstones along the Krušné hory Fault in northwestern Bohemia. The relationship between mineral chemistry and present and past fluid chemistry is also discussed. The studied samples come from the quarry of Jeníkov west of Teplice in the Eger Graben, ca. 4 km from its northern boundary fault.

Geological setting

Late Alpine epithermal mineralization is associated with the northern boundary fault of the graben — the Krušné hory Fault (Fig. 1). The oldest tectonic activity on the Krušné hory Fault dates back to the Oligocene-Miocene, but the largest movements are very young, extending beyond the Pliocene/Pleistocene boundary (Malkovský 1980; Coubal & Adamovič 2000). In the Jeníkov area, the total vertical displacement magnitude on the Krušné hory Fault is ~700 m (Malkovský 1980).

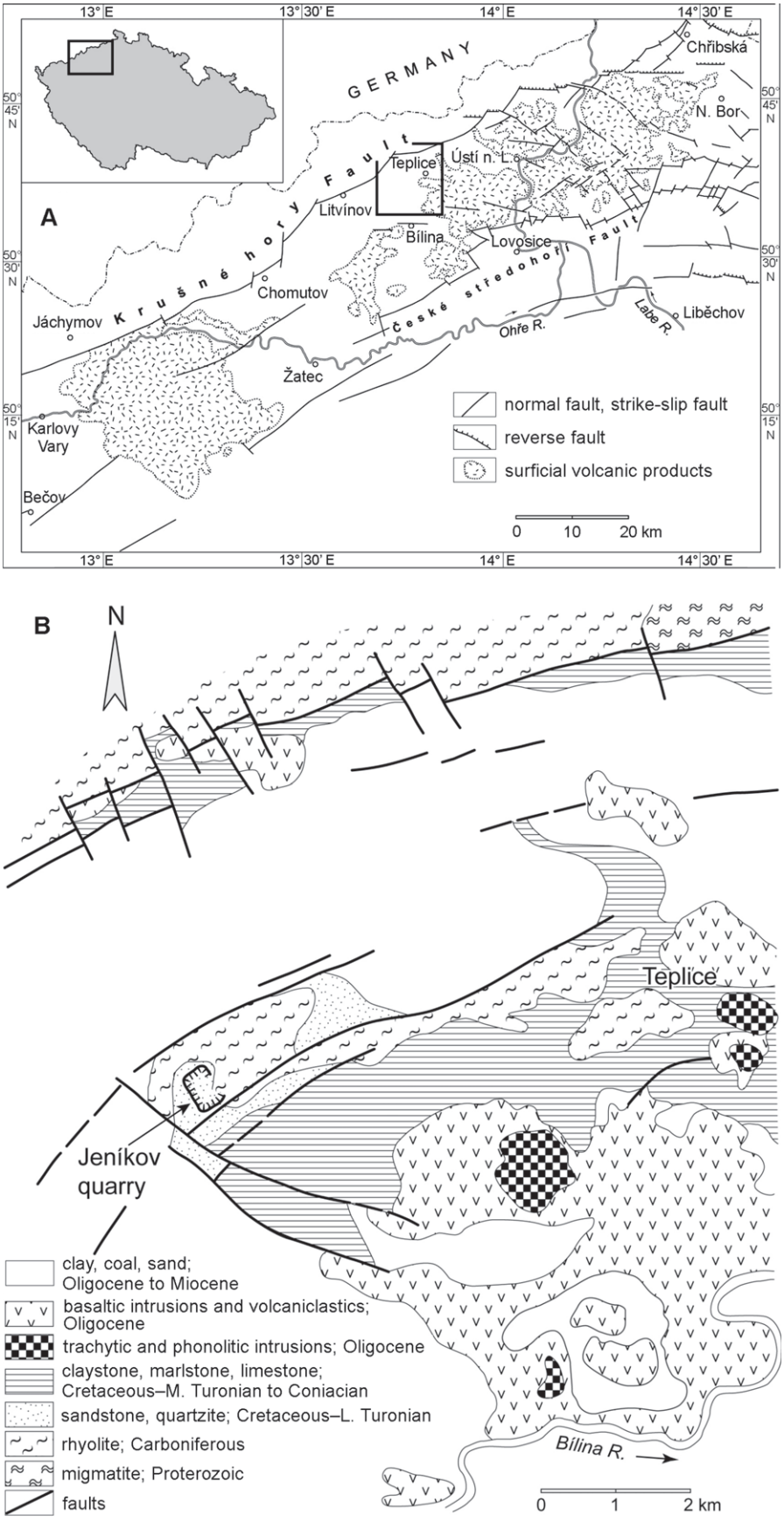

Fig. 1. A — A location map of the study area (frame) within the Eger Graben. **B —** A schematic geological map of the Jeníkov area.

Newly formed mineral phases are typically hosted by the Teplice rhyolite ignimbrite body and the overlying Cretaceous and Neogene detrital sediments. Three mineralization stages were recognized by Čadek et al. (1963): 1. silicification stage, 2. sulphidic stage with pyrite, marcasite, sphalerite and U oxides, and the youngest 3. barite-fluorite stage also characterized by Fe and U oxides, galena, sphalerite, pyrite etc. As for the character of fluids and ages of mineralization, the individual stages have been poorly constrained up to now. Barite and fluorite of stage 3, however, are clearly separated from stages 1–2 in time, and are compatible with the chemistry of the present thermal springs in the area.

Teplice rhyolite ignimbrite

The basement of the central part of the Eger Graben is formed by rhyolite ignimbrite of Carboniferous age, pertaining to the Altenberg-Teplice Caldera, extensively exposed in the adjacent part of the Krušné hory Mountains (e.g. Breiter 1997; Ulrych et al. 2006). A WSW–ENE-trending segment of the basement between Teplice and Jeníkov (Fig. 1), called the Teplice-Lahošť Ridge, functioned as a paleohigh in the pre-Late Cretaceous relief. Later, it was buried beneath Cretaceous marine sediments and beneath the Tertiary sedimentary and volcanic fill of the Eger Graben. Faulted boundaries of the Teplice-Lahošť Ridge suggest its tectonic uplift after the deposition of the Eger Graben fill. Rhyolite ignimbrite in its core became re-exposed to the surface by headward erosion of the Bílina River tributaries at approximately 500 ka (Čadek et al. 1964; Čadek & Malkovský 1968). Feldspar crystals in the rhyolite are sericitized and kaolinized. Dense joints are lined with bleached zones and covered with young mineral phases, notably hematite and quartz.

Upper Cretaceous sediments

In the central part of the Eger Graben, Cretaceous sediments have a stratigraphic range of Cenomanian to Coniacian, and a preserved thickness of max. 80 m. Most of the sedimentary package is formed by mud-dominated lithologies characterized by low permeabilities, not permitting effective fluid circulation.

Cenomanian sediments of continental/estuarine origin (Čech & Váně 1988) were deposited in topographic lows of the pre-Cenomanian relief only. They are arranged into upwards-fining cycles of conglomerate — arkosic sandstone — micaceous mudstone, and reach thicknesses of max. 20 m (Hrob area NW of Jeníkov).

Lower Turonian marine sandstones transgressively overlie the Teplice rhyolite. They reach a thickness of 7–25 m, wedging out towards the axis of the Teplice-Lahošť Ridge. The sandstone is massive or cross-bedded, composed of quartz with an admixture of feldspar and rhyolite fragments (< 3 %). Rhyolite boulders up to several meters in size are common immediately above the basal transgressive surface, together with coalified plant debris. Rhyolite granules to pebbles can be found near the top of the sandstone body, and locally concentrate into a bed of matrix-supported conglomerate. The amount of glauconite increases upwards in the topmost 2 meters. In the area between the Krušné hory Fault and the Teplice-Lahošť Ridge, Lower Turonian sandstones are pervasively cemented by secondary quartz. The amount of cement generally increases towards the top of the sandstone body. Silicified sandstones range from very light grey to dark grey in colour, depending on the proportion of sulphides (mostly pyrite) in the cement (Fig. 2a–c). A prominent peak in the content of sulphides occurs in the topmost 0.5 m (Fig. 3). Higher up, the silicified sandstones are unconformably overlain by Middle Turonian greyish brown mudstones and marlstones (Čech & Váně 1988) of very low primary permeability.

Structural controls on quartz cementation and sulphidic mineralization

Quartz cement is widely distributed in permeable detrital sediments of Cretaceous and Neogene age over a large area in the central Eger Graben, along the Krušné hory Fault. The highest intensity of quartz cementation is visible in areas where the sediments are directly underlain by the Teplice rhyolite and overlain by a low-permeability sealant rock. This suggests an advective fluid flow mediated by the dense network of fractures in the underlying rhyolite. Feldspar kaolinization along the flow paths could have served as a potential source of silica, as has already been demonstrated by Čadek & Malkovský (1968).

Brittle tectonic features in the silicified sediments of the central Eger Graben are more or less coeval with silicification but most of them clearly post-date the main silicification episode, as suggested by frequent striated fault planes in the cemented rock. This excludes a very young (Holocene) age for the main silicification episode. However, the silicification process must be younger than ~18 Ma, which is the age of the youngest preserved silicified strata (Burdigalian) along the Krušné hory Fault (Váně 1961). In the early stages, the advective/convective fluid flow could have been a thermally-driven process, connected with the Serravallian to Tortonian (13.4 to 9 Ma) volcanic activity in this part of the graben (Cajz 2000). However, no direct evidence has been reported.

The precipitation of fluorite and barite is clearly younger than the silicification process. Its Late Pliocene to Pleistocene age, coeval with the largest movements on the Krušné hory Fault and fault-scarp formation, is suggested by various lines of geological evidence (Čadek et al. 1963; Fengl 1995). These include the compatible chemistry of the present thermal waters in the area, the concentration of barite and fluorite occurrences in zones of modern groundwater issues, and their presence on joints dilated during the formation of the Krušné hory Fault scarp. In the Teplice area, timing of the barite mineralization can be constrained by the

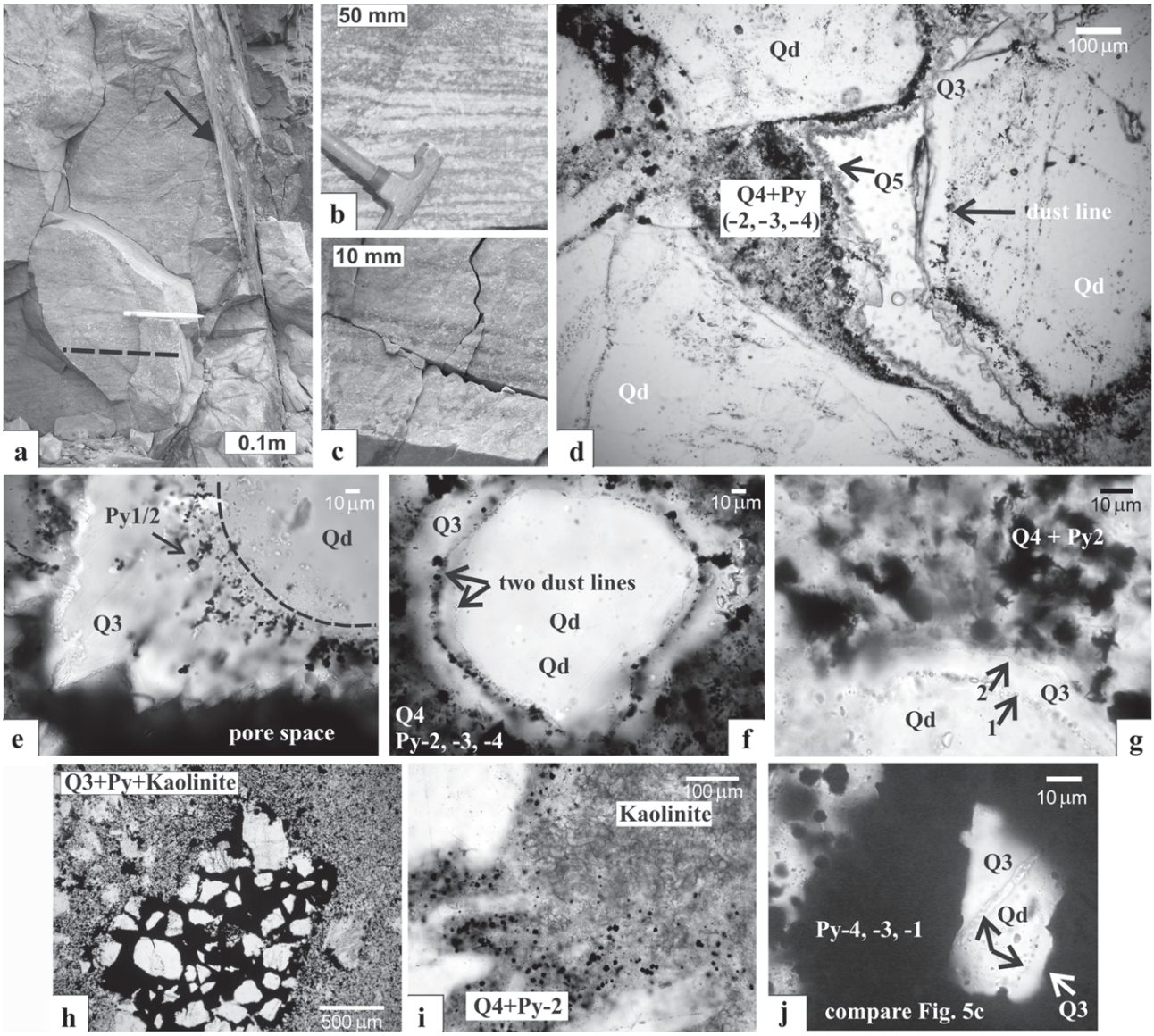

Fig. 2. a — A close-up view of silicified sandstones (quartzites). A subvertical fracture with sulphide impregnation along its walls is marked by an arrow. The strike of sulphidic impregnations, parallel to the original sandstone bedding, is highlighted by a dashed line. **b–c** — Examples of sulphidic impregnations parallel to sandstone bedding. **d–j** — Photomicrographs in transmitted light: d — Clasts of detrital quartz (Qd) rimmed by quartz overgrowths (Q3) with subordinate pyrite mineralization (Py-2, not labelled on the photo). Sandstone pores are partly filled with microcrystalline silica (Q4) with disseminated sulphides (Py-2, -3, -4). Pore spaces that were left free after Q4 and Py-2 to Py-4 precipitation were finally lined by crystals of late quartz (Q5). e — Early pyrite (Py-1/Py-2) trapped in quartz overgrowths (Q3). Pyrite precipitation partly postdates the onset of silicification (dustline formation). f — A quartz clast with two dustlines (indicated by arrows). Pyrite (Py-2) rims the outermost (intra-Qtz-3) dustline. Microcrystalline silica (Q4) and pyrites (Py-2 trough Py-4) fill the pores in sandstone. g — A detail of a quartz clast where Py-2 formation postdates quartz overgrowth formation (Q3). Numerous globules of framboidal Py-2, rimmed by laths of Py-2 intergrown with microcrystalline silica (Q4). h — Silica-sulphidic filling of an early fracture. Central part of the photo is occupied by an angular fragment of silicified (Q3) sandstone with pores completely filled with massive pyrite. i — A pore that was left free after Py-2 and Qtz-4 formation was later filled with kaolinite. j — Successive pyrite overgrowths (Py-1→Py-3→Py-4; see Fig. 5c for details) on a quartz clast (Qd) with a Qtz-3 (Q3) rim. Black arrows indicate the dust line.

exhumation of the Teplice-Lahošť Ridge (~500 ka; Čadek et al. 1964) but the youngest "radiobarites" are Holocene in age, as indicated by the disequilibrium between the activity of ^{226}Ra and the parent uranium in barite (Ulrych et al. 2007).

The REE patterns and uniform $\varepsilon_{Nd}(t)$ data close to zero for the fluorites from the Krušné hory Mountains show interaction of the mineralizing fluids with granites (Höhndorf et al. 1994). Fluid inclusion studies of sandstone-hosted vein fluorite indicated homogenization temperatures between 50 and 160 °C and transport by fluids of Na–HCO_3–Cl type (Höhndorf et al. 1994).

In the Jeníkov Quarry and its wider vicinity, no lateral variations in the intensity of silicification of Lower

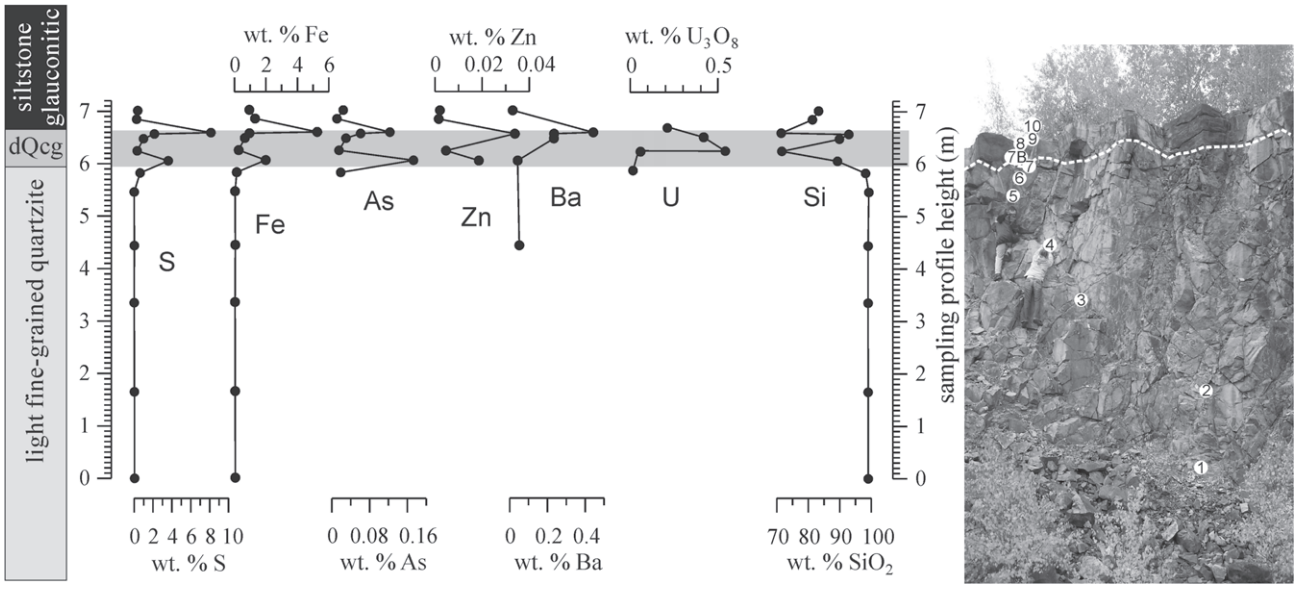

Fig. 3. Major and trace element contents in a section across Lower Turonian sandstones (quartzites). Analytical data correlate well with the visually remarkable sulphidic enrichment in the topmost 0.5 m of the quartzite. Sulphide (Fe, S) enrichment coincides with As, Zn, U and Ba enrichment. Sampling sites are shown on the inserted photo. The course of the sharp boundary between sulphide-enriched and sulphide-poor quartzites is highlighted by a white-dashed line. **dQcg** — dark coarse-grained quartzite.

Turonian sandstone have been observed. In contrast, disseminated sulphidic mineralization is visible in its southeastern sector only, that is above the apical part of the pre-Cretaceous rhyolite paleohigh. Sulphides in the Lower Turonian sandstones occur mostly disseminated (those that coprecipitated with the silica cement), less frequently fracture-related (Fig. 2a) and even enclosed in barite crystals lining the joint planes.

The study of successive generations of sulphides, spanning the period between the older silicification process and the young baritization, should therefore provide clues to the Pliocene, Pleistocene and Holocene fluid flow parameters in the late evolution of a rift basin.

Methods

Polished thin sections were prepared from about 20 samples of silicified sandstone from the Jeníkov Quarry. Sulphide textures and paragenetic relationships were studied by transmitted and reflected light optical microscopy and by the back-scattered electron mode (BSE) of electron scanning microscopy.

In order to study the intensity of pyritization in the quarry, 13 whole-rock samples each about 0.5–1 kg in weight were taken in a vertical section across the quartzites up to the sealing mudstone horizon (Fig. 3). After homogenization, the samples were analysed by XRF (Institute of Chemical Technology in Prague, J. Maixner and S. Randáková).

The chemistry of all pyrite generations was studied by the microprobe WD system (Cameca SX 100, Institute of Geology, AS CR, Prague). Elements measured: S (Ka), Fe (Ka), Co (Ka), Ni (Ka), Zn (Ka), As (La) and Tl (Mb). Spectrometers used: LTAP (As), LPET (Tl), PET (S), and LIF (Fe, Co, Ni). Standards used: marcasite (Fe, S), metallic Co (Co), metallic Ni (Ni), GaAs (As), ZnS (Zn) and TlBr (Tl). A total of 147 analyses were performed using the WD system.

The ED system (CamScan S4 microscope, Link ISIS 300 ED system, operator R. Procházka, Faculty of Science, Charles University in Prague, Prague) was used for a systematic study of Py-6 in barite from a wafer prepared for the study of fluid inclusions. Later, a thin section was prepared from the rest of the barite crystal, and a similar analytical profile was studied using the WD system. In total, 132 analyses were performed using the ED system.

Results

Schematic paragenetic relationships between individual primary minerals from the silicified Cretaceous sandstones at the Jeníkov Quarry are summarized in Fig. 4. In general two mineralization stages can be distinguished. The older, stage 1 comprises pervasive silica precipitation in the pores of sandstones, accompanied — and partly followed — by the precipitation of sulphides and minor uraninite. The minerals of stage 2, among which barite is the most frequent, and sulphides, uraninite and fluorite are less common, was typically precipitated on the walls of subvertical fractures (mostly NE-SW). Stage 2 is separated from stage 1 by a time gap during which most of the brittle deformation took place. In places, fractures whose formation coincided with late stage 1 are filled with microcrystalline quartz matrix with sulphidic and uraninite impregnations and with angular (breccia-like) fragments of

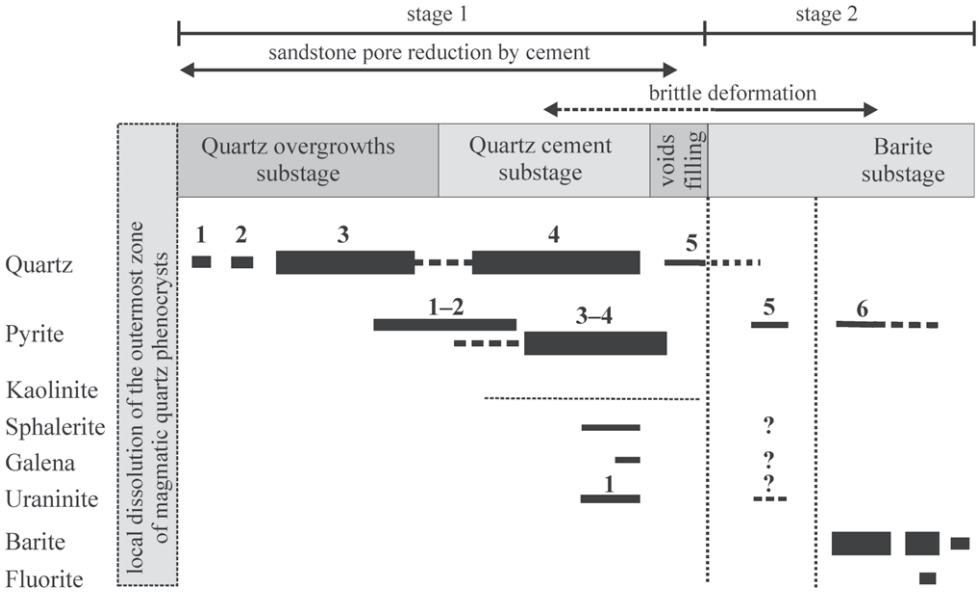

Fig. 4. Paragenetic relationships between primary minerals in silicified Cretaceous sandstones of the Jeníkov Quarry near Teplice, northern Bohemia.

silicified sandstone (Fig. 2h). Five generations of quartz were identified as products of sandstone silicification. Early silica formation has the character of euhedral quartz overgrowths (Qtz-1, Qtz-3) on detrital grains (Fig. 2e–g), rarely interspersed with scepter-like (Qtz-2) quartz crystal growth. Microcrystalline quartz cement (Qtz-4) and megaquartz crystals (Qtz-5) fill the remaining pores and voids in the rock (Fig. 2d,g–i). Six generations of pyrite (Py) were recognized, referred to as Py-1 (oldest) to Py-6 (youngest), and compared with the silicification products. Typically, the early ones (Py-1, -2) crystallized more or less together with the silica cement (Qtz-4) in the pores of Turonian sandstones (Fig. 2g), while the late ones (Py-3, -4, -5) fill the remaining pores and voids in the silicified sandstones, or joints and fractures in the rock (Py-5, -6; Fig. 5g). The main stage of pyrite formation (Py-2 and Py-3) generally postdates early silica formation (quartz overgrowths; Qtz-3; Fig. 2g). In some samples, however, the onset of pyrite precipitation is contemporaneous with the formation of late zones of quartz overgrowths (Qtz-3; Fig. 2e–f), that is it slightly precedes microcrystalline silica cement (Qtz-4). The timing of rare Py-1 (Fig. 5a–c) relative to the neoformed silica phases is disputable.

We have observed the following textural relationships between individual pyrite generations: i) Py-1→Py-3→Py-4 (Figs. 5a–c,f); ii) Py-2→Py-4 (Fig. 5d); iii) brittle-fractures related pyrites (Py-5→Py-6; Fig. 5g) are younger than the early ones (Py-1 to Py-4). The temporal relationship between Py-1 and Py-2 is based on indirect evidence only: on the presence of corrosion features in Py-1 and their absence in Py-2 and younger generations.

Representative microprobe analyses of pyrites of the different generations are given in Table 1.

Pyrite-1

Remnants of Py-1, exhibiting chemical corrosion features, were found in the cores of some Py-3 and Py-4 grains. No individual Py-1 grains were found. Py-1 relics are up to 80 ㎜ in size, corrosion is weak (Fig. 5a,c) to strong (Fig. 5b). Composite grains with pyrite relics typically fill pores in silicified sandstones, or less frequently imperfectly overgrow quartz clasts (Fig. 5c,f).

Py-1 is free of marked internal structures like As-rich or As-low bands on BSE images. Some grains, however, exhibit tiny micropores (Fig. 5a). Py-1 is almost stoichiometric FeS_2. A minor admixture of As (0.06 wt. %) was identified in one analysis only. The arithmetical mean and standard deviation of arsenic content is 0.01 ± 0.02 wt. % As (n = 6). No other elements were detected.

Pyrite-2

Py-2 forms framboids (~3 to ~70 ㎜ in size), mostly with disordered (Fig. 6b), less frequently with ordered (Fig. 6a; cubic close packing) internal structures. Individual pyrite crystallites form cubes (~0.5 to ~1 ㎜ in size), no octahedral ones were recorded. Framboids occur either isolated or in clusters consisting of up to 5 framboids. In contrast to Py-1, Py-2 lacks any corrosion features.

We further noticed a process of "welding" of individual pyrite crystallites within the framboids, the result of which are massive framboids with little pore space and with relatively large grains (Fig. 6c). Framboids are also frequently overgrown with pyrite (Py-4) cubes (~5 ㎜ in size; Fig. 6b and 6d), or laths (Fig. 6f).

The empirical formulae of Py-2 suggest a low anion surplus (S + As + Tl: 2.044–2.014) and a cation deficit (Fe: 0.956–0.986). Of trace elements, only arsenic was detected (0.11–0.60 wt. % As). The arithmetical mean and standard deviation of arsenic contents are 0.15 ± 0.04 wt. % As (n = 6).

Framboid size was measured systematically in two samples (Fig. 7). Sample JL-9B represents quartzite with disseminated sulphides from the most sulphide-rich zone of Lower Turonian sandstones just below (0–0.5 m) the

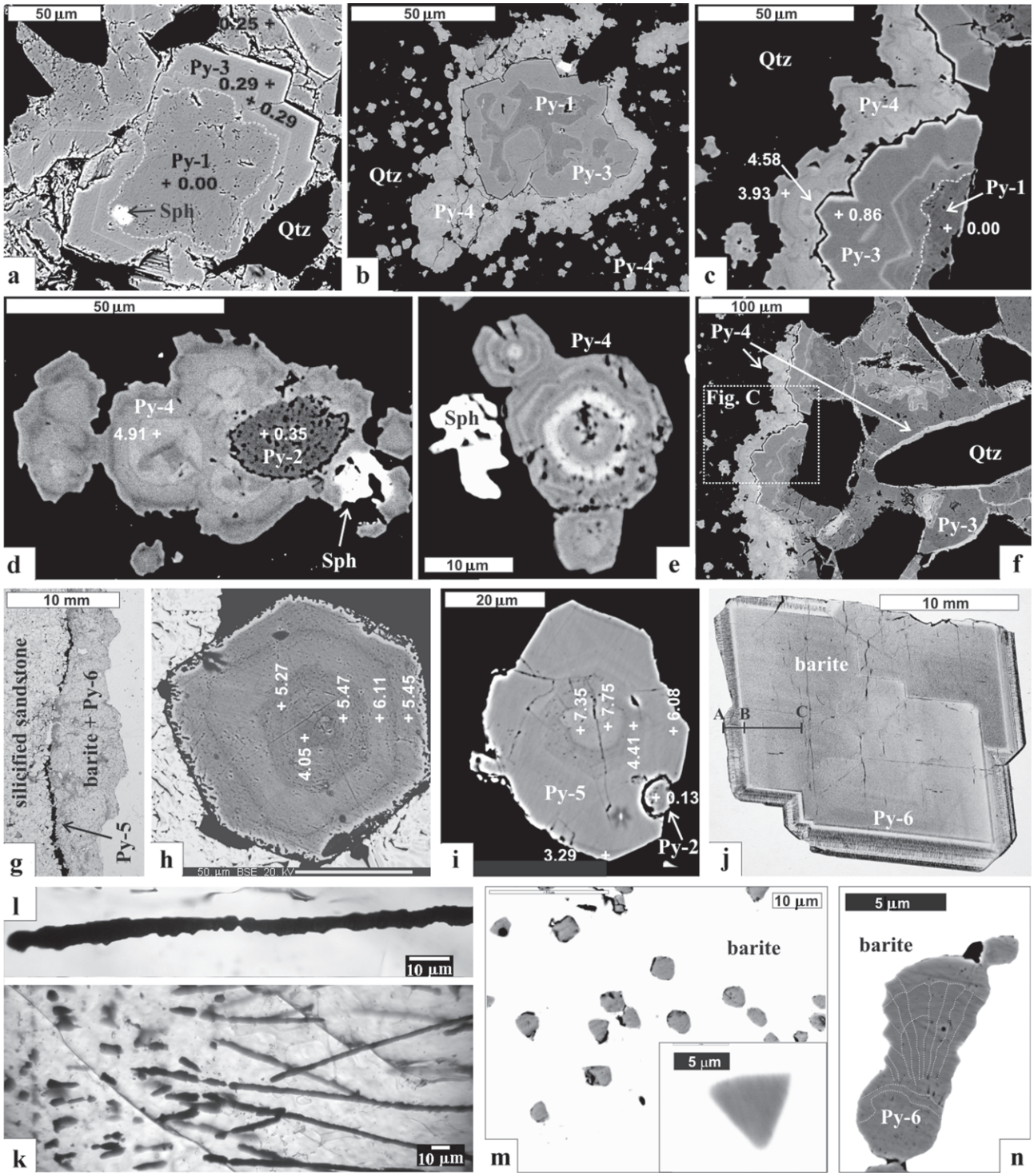

Fig. 5. Textures of the studied pyrites; crosses indicate sites of microprobe analyses; numbers refer to As wt. %; Sph = sphalerite: **a** — corroded Py-1 relics enclosed by a Py-3 grain (BSE image); **b** — intensively corroded Py-1 grain enclosed in Py-3 and overgrown by Py-4; **c** — Py-1 relics growing on a quartz grain with Qtz-2 overgrowths (BSE); **d** — Py-4 aggregate enclosing framboidal pyrite (Py-2; BSE); **e** — euhedral Py-4 grain with several As-rich oscillation growth zones (BSE); **f** — complex grain with Py-4 overgrowth and fracture fillings (BSE); **g** — fracture in silicified sandstone with coatings of Py-5 and a younger barite filling (transmitted light); **h–i** — As-rich Py-5 grains (BSE); **j** — a barite crystal (section parallel to 010 ??) with a large unzoned core and compositionally zoned rim. Line A–B–C marks the position of the microanalytical profile where Py-6 chemistry was studied (transmitted light); **k** — a part of barite rim showing composite Py-6 needles (transmitted light); **l** — a detailed view of a Py-6 needle composed of tens of individual Py-6 crystals (transmitted light); **m** — Py-6 crystals from the core of barite crystal (BSE); **n** — a detail of a Py-6 lath/needle from the outermost growth zone exhibiting complex fan-like textures (marcasite?; BSE).

Table 1: Representative microprobe (WDX) analyses of the studied pyrites and numbers of atoms per formula unit calculated to 3 positions (n.d. — not detected).

Sample	JL20A	JL20A	JL9B	JL9B	JL7A	JL20A	JL20A	JL20A	JL7A	JL20A	JL20A
analysis	22	24	27	28	101	29	33	41	111	122	130
type	Py-1	Py-1	Py-2	Py-2	Py-2	Py-3	Py-3	Py-4	Py-4	Py-4	Py-4
Fe	46.53	46.76	46.19	47.63	45.76	46.51	46.41	44.65	45.23	44.31	45.11
As	0.00	0.06	0.11	0.17	0.16	0.31	0.17	4.52	2.90	5.83	4.48
S	53.14	53.10	54.11	52.29	53.67	53.15	53.30	50.70	51.67	49.40	49.99
Co	n.d.	n.d.	n.d.	n.d.	n.d.	n.d.	n.d.	n.d.	n.d.	n.d.	n.d.
Ni	n.d.	n.d.	n.d.	n.d.	n.d.	n.d.	n.d.	n.d.	n.d.	n.d.	n.d.
Zn	n.d.	n.d.	n.d.	n.d.	n.d.	n.d.	n.d.	n.d.	n.d.	n.d.	n.d.
Tl	n.d.	n.d.	n.d.	n.d.	n.d.	n.d.	n.d.	n.d.	n.d.	n.d.	n.d.
TOTAL	99.67	99.92	100.41	100.09	99.58	99.97	99.88	99.87	99.79	99.54	99.57
Fe	1.004	1.007	0.986	1.029	0.985	1.002	0.999	0.983	0.988	0.987	0.999
As	0.000	0.001	0.002	0.003	0.003	0.005	0.003	0.074	0.047	0.097	0.074
S	1.996	1.992	2.012	1.968	2.012	1.994	1.998	1.943	1.965	1.916	1.927
Co	0.000	0.000	0.000	0.000	0.000	0.000	0.000	0.000	0.000	0.000	0.000
Ni	0.000	0.000	0.000	0.000	0.000	0.000	0.000	0.000	0.000	0.000	0.000
Zn	0.000	0.000	0.000	0.000	0.000	0.000	0.000	0.000	0.000	0.000	0.000
Tl	0.000	0.000	0.000	0.000	0.000	0.000	0.000	0.000	0.000	0.000	0.000
TOTAL	3.000	3.000	3.000	3.000	3.000	3.000	3.000	3.000	3.000	3.000	3.000
S+As+Tl	1.996	1.993	2.014	1.971	2.015	1.998	2.001	2.017	2.012	2.013	2.001
Fe+Co+Ni	1.004	1.007	0.986	1.029	0.985	1.002	0.999	0.983	0.988	0.987	0.999

Sample	JL9B	JL7A	JL7A	JL7A	JL25D	JL25D	JL25D	JL25D	JLB-1	JLB-1	Ul-13
analysis	37	105	106	107	91	93	95	143	72	52	45
type	Py-4f	Py-4f	Py-4f	Py-4f	Py-5	Py-5	Py-5	Py-5	Py-6	Py-6	Py-6
Fe	44.61	44.89	45.03	45.51	44.12	44.56	44.03	45.01	31.77	44.90	30.33
As	5.47	3.14	3.81	1.16	7.49	5.15	7.96	4.41	0.17	0.56	0.01
S	50.93	52.13	51.12	53.25	48.63	50.53	48.06	50.76	53.02	53.22	53.36
Co	n.d.	n.d.	n.d.	n.d.	n.d.	n.d.	n.d.	n.d.	8.81	n.d.	12.02
Ni	n.d.	n.d.	n.d.	n.d.	n.d.	n.d.	n.d.	n.d.	5.89	n.d.	3.98
Zn	n.d.	n.d.	n.d.	n.d.	0.00	0.00	0.00	n.d.	0.00	0.00	0.00
Tl	n.d.	n.d.	n.d.	n.d.	0.08	0.07	n.d.	0.02	n.d.	0.34	n.d.
TOTAL	101.01	100.16	99.95	99.92	100.33	100.30	100.05	100.20	99.67	99.02	99.71
Fe	0.974	0.976	0.987	0.981	0.985	0.980	0.988	0.988	0.690	0.975	0.657
As	0.089	0.051	0.062	0.019	0.125	0.084	0.133	0.072	0.003	0.009	0.000
S	1.937	1.973	1.951	2.000	1.890	1.935	1.879	1.940	2.005	2.014	2.014
Co	0.000	0.000	0.000	0.000	0.000	0.000	0.000	0.000	0.181	0.000	0.247
Ni	0.000	0.000	0.000	0.000	0.000	0.000	0.000	0.000	0.122	0.000	0.082
Zn	0.000	0.000	0.000	0.000	0.000	0.000	0.000	0.000	0.000	0.000	0.000
Tl	0.000	0.000	0.000	0.000	0.001	0.000	0.000	0.000	0.000	0.002	0.000
TOTAL	3.000	3.000	3.000	3.000	3.000	3.000	3.000	3.000	3.000	3.000	3.000
S+As+Tl	2.026	2.024	2.013	2.019	2.015	2.020	2.012	2.012	2.007	2.025	2.014
Fe+Co+Ni	0.974	0.976	0.987	0.981	0.985	0.980	0.988	0.988	0.993	0.975	0.986

sealing horizon of Middle Turonian claystones. Sample JL-15 comes from a fracture with sulphides in otherwise sulphide-free quartzite. This sample is located about 150 m to the NW away from the most sulphide-rich zone and stratigraphically about 4–5 m below the Lower/Middle Turonian boundary. Both data show lognormal distribution of similar standard deviations, but of significantly different median values (~12 μm and ~30.5 μm for JL-9B and JL-15, respectively). Data from other, less systematically studied samples, are similar to those from JL-9B.

Pyrite-3

Py-3 forms crystal-faced overgrowth zones on Py-1 (Fig. 5a–c,f). It is homogeneous on BSE (0.17–39 wt. % As), except for 1 or 2 thin (~1–2 μm) As-rich growth bands (4.11 wt. % As). The arithmetical mean and standard deviation of arsenic contents are 0.31 ± 0.20 wt. % As (n = 12). No other trace elements were detected.

Pyrite-4

Py-4 forms euhedral overgrowths on the Py-3 to Py-1 surfaces (Fig. 5b–d) and/or individual grains (cubes max. 50 μm in size; Fig. 6b–d,e), disseminated in (intergrown with?) fine-grained silica cement (Qtz-4).

The overgrowths typically consist of several thick As-rich zones separated by thin (~1–2 μm) As-poor bands (Fig. 5c–d). Numerous As-poor patches located close to the base of Py-4 overgrowths most probably represent crystallization seeds/centres. Individual pyrite grains/

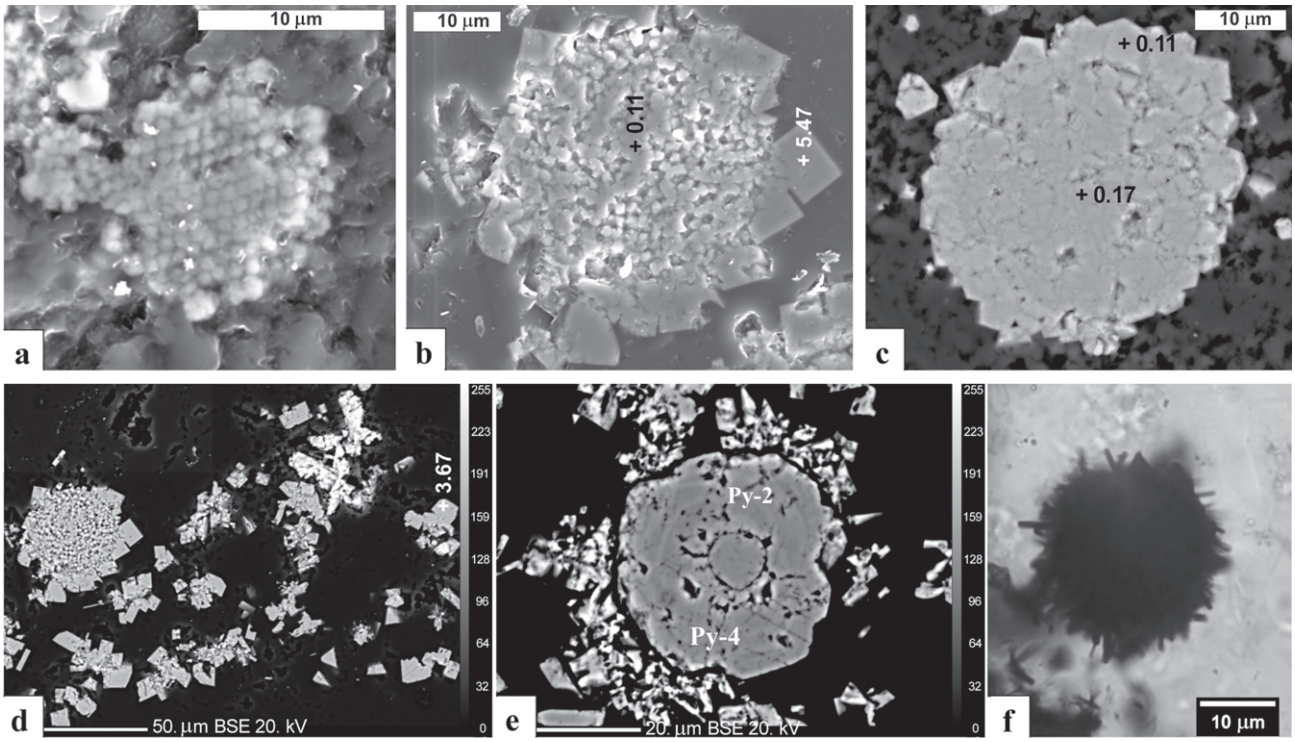

Fig. 6. Various framboid textures. Crosses indicate sites of microprobe analyses. Numbers refer to As wt. %. **a** — a framboid cluster with cubic closely packed internal structure (BSE image); **b** — a framboid with disordered texture and Py-4f cube overgrowths; **c** — a "welded" framboid approaching massive texture (BSE); **d** — a framboid overgrown with Py-4f and isolated Py-4f crystals (BSE); **e** — framboid relics in the core of a Py-4 grain (BSE); **f** — a framboid globule overgrown with Py-4 laths (transmitted light).

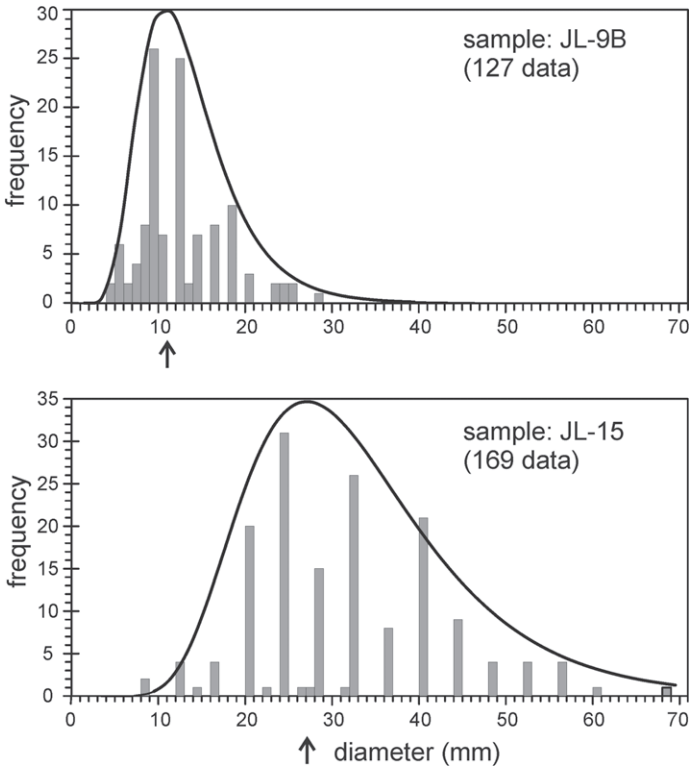

Fig. 7. Frequency distribution of framboid size in two samples, both exhibiting lognormal data distribution.

zones exhibit similar textures. Py-4 rarely encloses/overgrows small (up to 20 μm) grains of sphalerite or galena.

Arsenic admixture is high (2.16–6.62 wt. % As), but nickel and cobalt were below detection limits. The arithmetical mean and standard deviation of arsenic contents are 3.91 ± 1.64 wt. % As (n = 24). Thallium was found in some grains only, ranging from 0.01 to 0.12 wt. %.

In some samples, we have found BSE-homogeneous pyrite cubes (isolated or overgrowing Py-2 framboids; Fig. 6b–e) with high As contents (2.94 ± 1.46 wt. % As; n = 8) similar to those in typical Py-4.

Pyrite-5

Py-5 forms massive coatings on post-silicification fractures (where it is overgrown by barite with Py-6; Fig. 5g) or individual grains up to 80 μm in size in the pores of silicified sandstone in the vicinity of these fractures.

Py-5 grains frequently exhibit a crystallization core, consisting of one or more As-rich grains (Fig. 5h–i) and a massive thick overgrowth zone. Small variations in the As/S ratio can be found in the overgrowths (Fig. 5h). In contrast to Py-3 and Py-4, all growth zones (including grain cores) are extremely As-rich (4.05–7.96 wt. % As). The arith-

metical mean and standard deviation of arsenic contents are 6.14 ± 1.10 wt. % As (n = 29). Thallium contents range between 0.0 and 0.082 wt. %; arithmetical mean and standard deviation correspond to 0.05 ± 0.02 (n = 17). No nickel or cobalt admixtures were detected.

Pyrite-6

Py-6 forms numerous tiny (max. 10 mm; Fig. 5m–n) crystal inclusions in barite crystals that precipitated in late fractures in the quartzites. Rows (lines) of single Py-6 inclusions typically rim individual barite growth zones (Fig. 5j). Only those from the latest, or several latest, growth zones are commonly arranged in needles, consisting of welded single crystals (Fig. 5k–l). In rare cases, an amorphous carbon phase was identified associated with these needle-shaped Py-6 crystals.

Significant variations in the pyrite trace element chemistry were recorded along the profile across several barite growth zones (Fig. 8a): the oldest Py-6 inclusions are variably enriched in Ni (3.47 ± 2.09 wt. %), Co (8.86 ± 3.68 wt. %) with traces of As and Zn, while the younger ones are only slightly enriched in arsenic (0.76 wt. % As). The transition zone at the boundary between Ni-Co-rich core and Ni-Co-free rim is marked by a sudden increase in arsenic content (up to 4 wt. % As; restricted to one growth zone only). The arithmetical mean and standard deviation of arsenic contents are

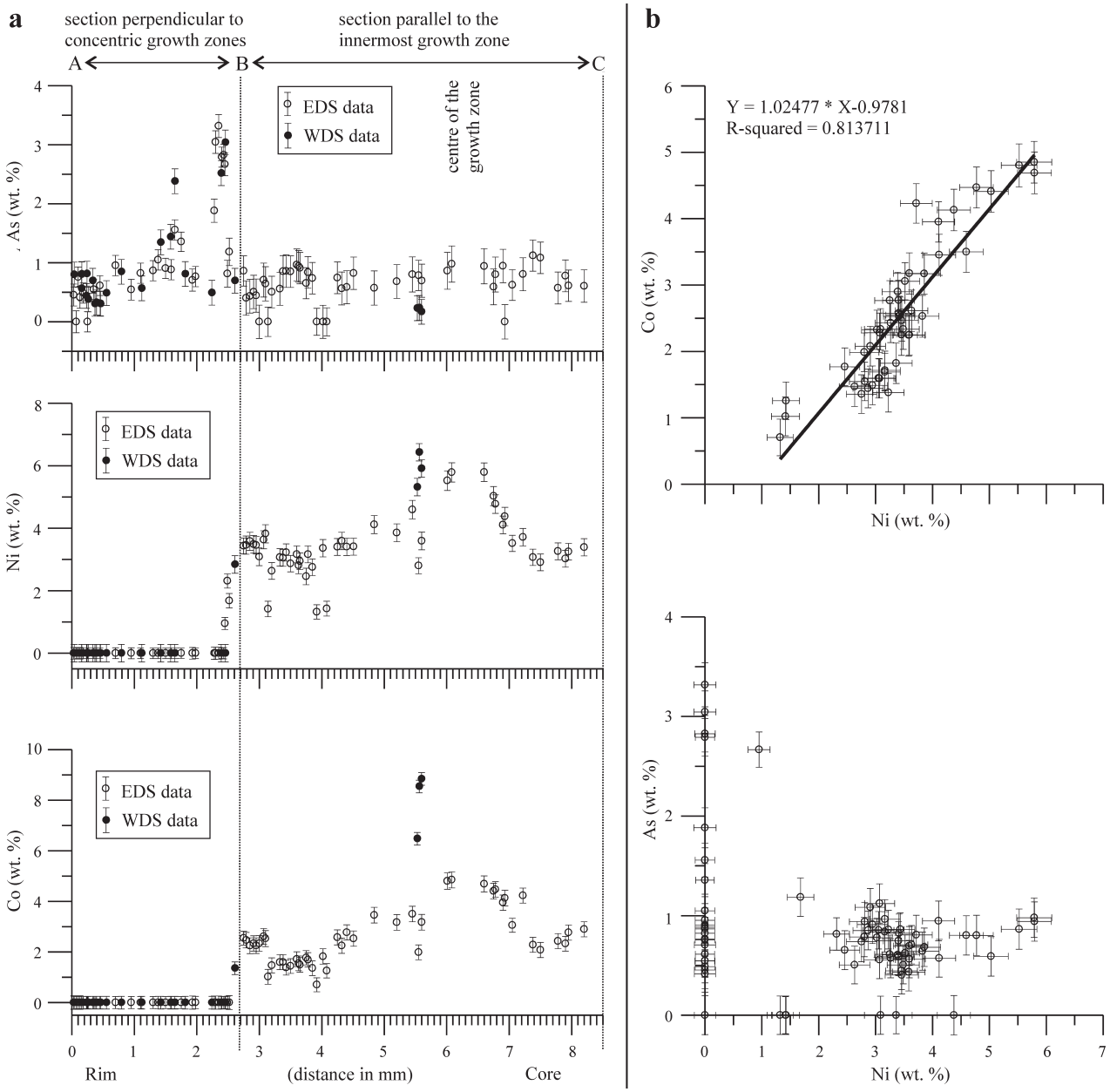

Fig. 8. Chemistry of Py-6 inclusions from a barite crystal: **a** — systematic variations in Py-6 crystals along the studied profile A–B–C (Fig. 5j); **b** — a correlation of Co-Ni and As-Ni contents from Py-6.

0.76 ± 0.71 wt. % As (n = 33). Py-6 is the most thallium-rich generation 0.19 ± 0.13 wt. % Tl (n = 15; mean ± SD), although Tl was not detected in all studied Py-6 grains.

Trace element chemistry of pyrites — a summary

Individual pyrite generations/types differ significantly in arsenic content (average As contents: 0.01, 0.15, 2.94, 3.91, 6.14 and 0.76 wt. % As for Py-1 through Py-6, respectively; Fig. 9) that gradually increases towards younger pyrite types (except for Py-6). Arsenic contents in most of the analysed Py-1 and Py-2 grains were below the detection limits.

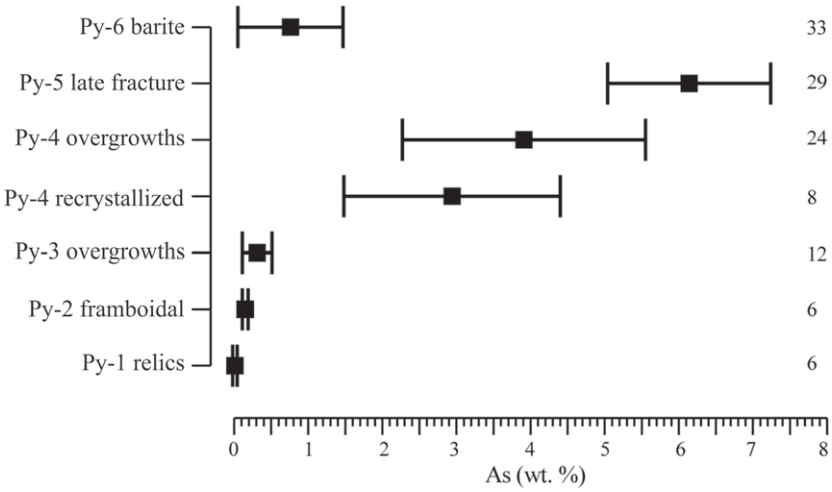

Fig. 9. A summary of arsenic admixture statistics (arithmetical mean and standard deviation) for the studied pyrites.

Arsenic contents correlate well with sulphur deficit, suggesting $As_{+1}S_{-1}$ substitution mechanism (Fig. 10a). No correlation exists between Ni or Co and As contents in Py-6 grains, but it does exist between the Ni and Co contents themselves (Fig. 8b) for pyrite inclusions in the studied barite crystal (Fig. 5j). We have further noticed a tendency for slight iron deficiency (Ni and Co were below detection limits in most analysed grains) with gradually increasing arsenic content (Fig. 10). This trend, however, is not statistically well documented, because of the given standard deviation for iron contents. True occupancy of pyrite structural sites therefore remains to be proved by the single crystal X-ray method.

Discussion

Relationships of pyrite types to silicification processes

Mutual textural relationships clearly indicate that Py-1 to Py-4 (±Py-5 ?) pyrite types formed as a consequence of one complex mineralization process, accompanying widespread silicification in the Jeníkov-Lahošť (Teplice) area. Py-1 relics likely do not represent pre-silicification pyrite, but postdate the onset of silicification. This can be deduced from Py-1 overgrowths on quartz clasts with neoformed silica (Qtz-3) overgrowth rims (Figs. 2j and 5c). Py-2 (framboids) precipitated largely in the pores of sandstone, together with microcrystalline quartz cement (Qtz-3). The same is true for Py-3 and Py-4. Py-5 postdates the main silicification stage (Qtz-2, -3) only. The continuity in arsenic content from Py-4 to Py-5 and the contrast in arsenic content between Py-5 and Py-6 allow us to suggest that Py-5, although texturally postdating silicification (filling fractures in already silicified sandstone; Fig. 5g), is still genetically related to the silicification process. Py-1 to Py-5 therefore represent a single more or less continuous evolution of pyrite crystallization. Py-6, having the form of

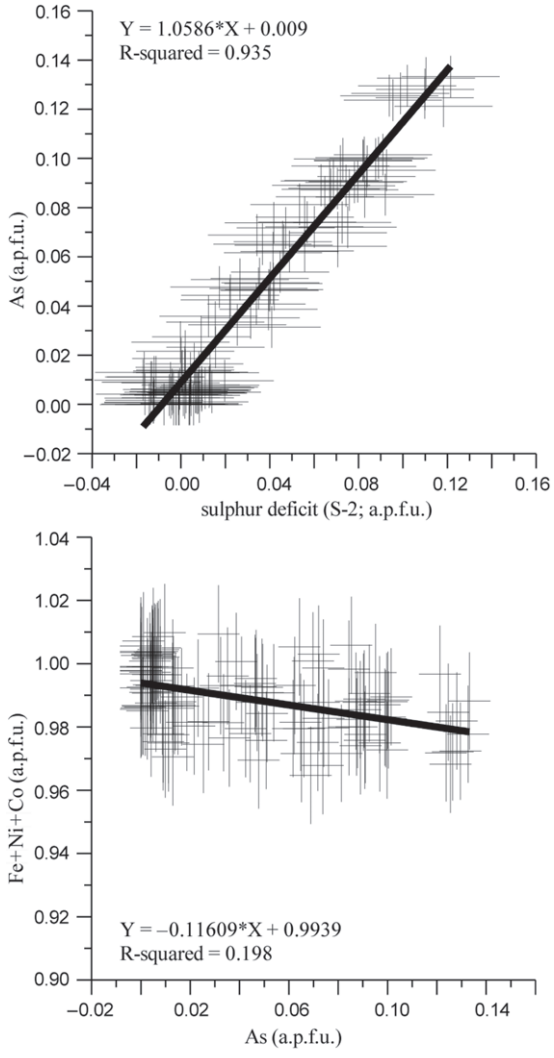

Fig. 10. Correlation of the arsenic admixture in pyrites with: **a** — sulphur deficiency — indicating $As_{+1}S_{-1}$ substitution mechanism; **b** — cation deficiency (mostly iron deficiency).

inclusions in late tabular barite crystals, is probably separated by a time gap from the previous types. The duration of this pyrite evolution gap is difficult to assess, but the youngest growth zones of barite crystals are Holocene in age (Ulrych et al. 2007).

The actual temperatures of the above mentioned silicification are not known but the presence of only one-phase liquid fluid inclusions (sparse at Jeníkov, but more frequent at Salesiova výšina Hill, approximately 5 km from Jeníkov) in quartz overgrowths (Qtz-3) and on dustlines separating quartz clasts and overgrowths allow us to suggest temperatures not exceeding approx. 50–60 °C.

Similar temperatures (~53 °C) were estimated by Hladíková et al. (1979) for the formation of calcite veinlets (fracture fillings) from the Teplice area (suggesting $\delta^{18}O_{water}$: –10‰ SMOW, similar to the present-day groundwater).

The present-day temperature of mineralized thermal waters at Teplice, a likely analogue for the fossil fluids, is 32–49 °C (Čadek et al. 1968). When the present chemistry of thermal waters (Čadek et al. 1968; analyses 1–3, 28 from table 24) is used, then the "fluid reservoir" temperatures estimated from various empirical chemical thermometers correspond to: ~88 °C (SiO_2, quartz; Fournier & Potter II 1982), ~57 °C (SiO_2, chalcedony; Table 6.1 in Kharaka & Mariner 1989), ~96 °C (Na–K–Ca; Fournier & Truesdel 1973), and ~65 °C (Mg–Li; Kharaka & Mariner 1989). Na-K as well as Na-Li thermometers yielded unrealistically high temperatures (160–210 °C).

All these data unequivocally point to a low-temperature (~50 °C) origin of the studied pyrites and associated mineralizing fluids.

Solubility of arsenic, nickel and cobalt in pyrite

The solubility of arsenic solid solution in pyrite/marcasite at low temperatures is difficult to study experimentally. Contents of up to ~19 wt. % As were recorded in some natural hydrothermal pyrites formed at temperatures lower than 300 °C (Reich & Becker 2006 and references therein). Recent thermodynamic calculations of Reich & Becker (2006) restricted the solubility of arsenic in pyrite to about ~2.1, ~2.7 and ~6 wt. % As at ~25, ~100 and ~500 °C, respectively. Concentrations exceeding such ranges correspond either to metastable arsenic solid solution, or suggest a presence of arsenopyrite nanoscale domains in the pyrite structure.

Of the studied pyrites, average As contents (Fig. 9) in Py-2, -3 and -6 are compatible with a stable arsenic solid solution according to Reich & Becker (2006), while those of Py-5 exceed this limit. Arsenic contents in Py-4 oscillate around this limit.

As the arsenic content in Py-6 does not exceed the theoretical limit for arsenic solubility in pyrite at 25 °C (Reich & Becker 2006), we may suggest the same for nickel and cobalt. Experimental or theoretical data for solubility of cobalt and nickel in pyrite formed at subambient temperatures are missing. Klemm (1965) suggested solubilities of about 10 at. % of CoS_2 or NiS_2 in FeS_2 at 400 °C.

Constraints on fluid saturation with respect to iron and sulphur

Numerous experimental studies (Ohfuji & Rickard 2005 and references therein) demonstrated that major prerequisites for framboid formation are 1. extremely high supersaturation with respect to iron sulphides and 2. conditions when crystal nucleation rate significantly exceeds the crystal growth rate. These favourable conditions may result from increasing/higher fluid temperature (>150 °C), from the presence of small amounts of O_2 in the system, from the presence of S(0) and polysulphides, or from increasing Eh.

Of these factors, Eh variations are the most likely factor at Jeníkov. An increase in Eh can be indirectly deduced from the presence of isolated cogenetic inclusions of $FeOOH–FeS_2$ and/or siderite enclosed in quartz overgrowths (Qtz-3) at Salesiova výšina Hill. Due to much steeper decrease of pyrite solubilities along the $FeS_2–FeOOH$ or $FeS_2–Fe^{2+}$ phase boundary than along other pyrite boundaries (Fig. 11a), a slight Eh increase coupled with a subtle increase in pH is the most effective way to produce fluids highly supersaturated with respect to iron sulphides, thus initiating framboid formation (cf. fig. 3 of Butler & Rickard 2000).

The presence of welded framboids (Fig. 6c), where crystallites have grown at the expense of micropores, reflects conditions when pyrite growth rate exceeded that of nucleation. The same can be inferred from the absence of framboid structures in later pyrite types (Py-3, -4, -5). Relatively fast nucleation also accompanied later Py-4, as shown by the chaotic BSE textures with numerous nucleation centres (Fig. 5c–e), but not enough for framboid formation.

Processes that led to a partial dissolution of early pyrite (Py-1), notably the time gap between Py-1 dissolution and Py-2 formation, are more obscured. If we accept that Py-1 postdates the early silicification phase, then the formation and dissolution of Py-1 came only a short time before the Py-2 (framboid) formation. With regard to the kinetics of pyrite oxidation (Williamson & Rimstidt 1994), a short-lived and fast pyrite dissolution requires a sudden high increase in the amount of dissolved oxygen (e.g. by the factor of 10^5–10^6 to increase the half-times of pyrite dissolution by the factor of 300× to 1000×; based on the rates of Williamson & Rimstidt 1994). To allow Py-2 formation in the next step, a return to reducing conditions is necessary, followed by a less dramatic increase in oxygen activity to promote pyrite supersaturation and framboid formation (see above). Later, when Py-3 to Py-5 are formed, conditions in the stability field of pyrite can be expected again. The observed mineral association thus reflects oscillatory changes in the oxygen activity of the mineralizing fluids, gradually diminishing with time (Fig. 11b). With regard to the more or less neutral pH of fossil and present thermal waters, dissolved oxy-

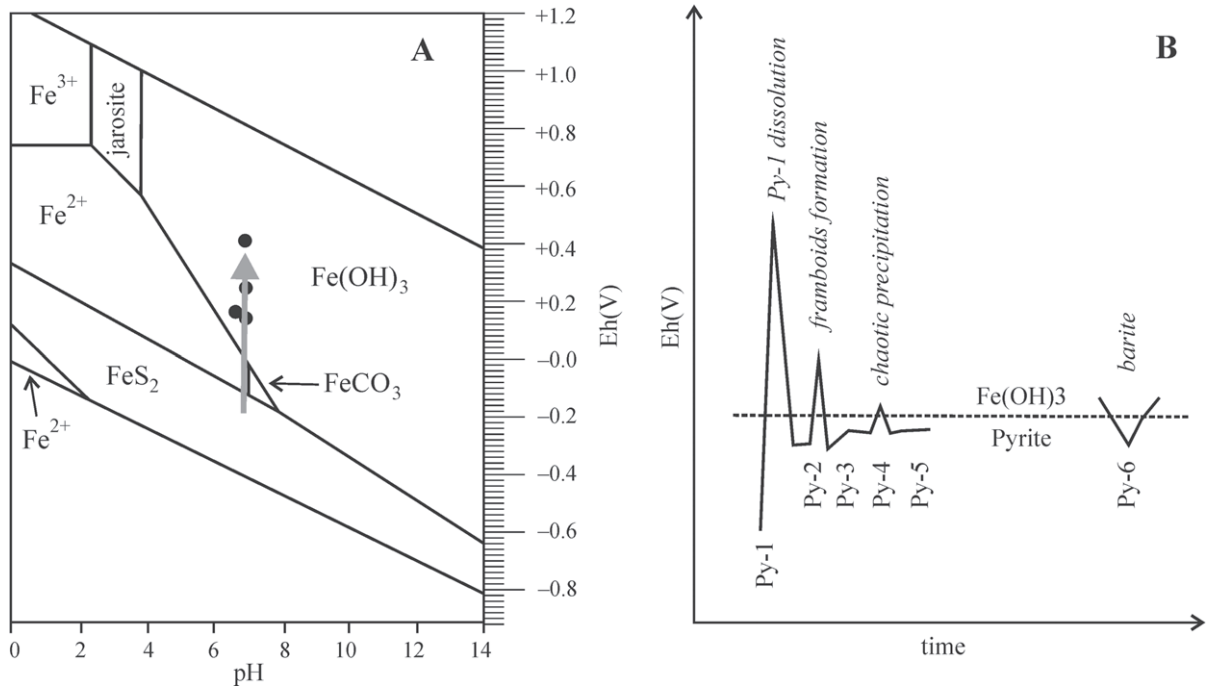

Fig. 11. Relationships between fluid chemistry and mineralogy: **a** — Eh-pH diagram for the system Fe-K-S-CO_2-H_2O-O_2 at 25 °C, 1 bar pressure, $\Sigma Fe(aq) = 10^{-4}$ mol/kg, $\Sigma K(aq) = 10^{-4}$ mol/kg, $\Sigma S(aq) = 10^{-2}$ mol/kg and $P_{CO_2} = 10^{-2}$ bar (after Nordstrom & Munoz 1985 in Langmuir 1996) with dots indicating the chemistry of the present thermal waters from the Teplice area. Note that the thermal waters are far from equilibrium with iron sulphides. The observed mineralogy (pyrite, siderite, uraninite, iron oxyhydroxides) is compatible with increasing Eh (thick arrow) under pH similar to present-day thermal waters. **b** — schematic changes in Eh with time, necessary to produce the observed variations in pyrite textures.

gen is the most likely agent for pyrite oxidation. Hydroxyl radicals ($HO^{\bullet}$), or H_2O_2 produced by radiolysis of water (Lefticariu et al. 2006) represent a less probable alternative to dissolved oxygen.

Framboids formed under euxinic conditions in modern basins tend to be smaller and less variable in size than those formed under dysoxic conditions (Wilkin et al. 1996). The dependence of mean framboid size on the oxygen fugacity probably also exists at Jeníkov. Framboids from the zone of most intense pyritization immediately underlying the mudstone sealing horizon are smaller than those from more distal places, where the fluids could mix with other more oxidized groundwaters, or where the role of exhaustion of reducing components in the parent fluid was becoming important.

Chemistry of present-day thermal waters in the Teplice area

The thermal waters at Teplice have been monitored for more than 100 years. Despite changes in instrumentation, the results of major cation chemistry and pH measurements are comparable over this whole period: pH: 6.6–6.9, Eh: +0.137 to +0.202 V and +0.410V, SiO_2: 27–49 mg/l, Na: 160–240 mg/l, K: 10–18 mg/l, Ca: 35–110 mg/l, total sulphur as SO_4^{2-}: 83–136 mg/l, $HAsO_4^{2-}$: 0.01 mg/l (Čadek et al. 1968 and unpublished recent analyses). The sampled waters, however, do not represent a pure thermal water end-member, as mixing with shallow groundwater occurs just beneath the discharge zone.

Mineral saturation indices (SI) were calculated using PhreeqC (Parkhurst & Appelo 1999) and thermodynamic database minteq.v4 in order to evaluate the saturation of present-day thermal waters with respect to the mineral of interest: pyrite is strongly undersaturated (SI: over –90), siderite is slightly undersaturated (SI: –4 to –10), barite and quartz is more or less in equilibrium with the waters (SI: –0.6 and 0.7, respectively), kaolinite and goethite are slightly supersaturated (SI: 2 to 5). Fossil waters responsible for sulphidic mineralization could have pH values similar to those of present-day thermal waters, but must have had a distinctly lower Eh.

The evolution of fluid trace element chemistry and changes in fluid migration paths

The trace element chemistry of minerals can be used as a paleoindicator of fluid chemistry, species activities, and the degree of saturation. As stated earlier, all pyrite types precipitated at similar temperatures, with differences not exceeding 20–30 °C. The influence of temperature as a factor governing As, Ni, Co and Tl contents in pyrites can therefore be ruled out. The As (Ni, Co, Tl) admixture in pyrites likely reflects the contents/saturation of these elements in fossil fluids. The effect of variations in the trace element contents in the

mineralizing fluids on the pyrite chemistry was confirmed and discussed in the study on uraninite, which co-precipitated with Py-4 (Zachariáš et al., in prep.). Besides element contents in the fluid phase, kinetics of pyrite precipitation could also contribute to the formation of As-rich and As-poor pyrite growth zones.

Arsenic contents in fluids at the site of fluid discharge can result from two different interactions (besides the role of temperature): i) from As-saturation/depletion due to precipitation of various As-bearing compounds at, or close to the discharge site (e.g. Cleverley et al. 2003); or ii) from complex fluid-rock interactions governed by actual As-minerals (usually arsenopyrite or As-pyrite) in a deep fluid reservoir at temperatures appropriate for this reservoir (e.g. Aiuppa et al. 2006). Fluid boiling in a deep reservoir, or fluid evaporation at the site of surface discharge, would also result in a gradual increase in arsenic content in the remaining liquid phase; but, these processes are difficult to demonstrate in our case. Because the As-bearing pyrite is the only As-bearing mineral at Jeníkov, the process of fluid saturation/depletion by As due to precipitation of various As-bearing compounds can be neglected. The gradual increase in As contents from Py-1 to Py-5 therefore most probably reflects a gradual increase in As content in the parent fluid.

Such a trend indicates fluid-rock interactions in a deep crystalline reservoir at progressively increasing temperatures and depths and/or progressively opening fluid migration paths. Temporal coincidence of pyrite formation with large-scale movements along the Krušné hory Fault suggests a fault-driven upward transport of fluids either by the mechanism of solitary waves of Revil & Cathles (2002) or some type of seismic pumping (e.g. Sibson et al. 1975).

As has been stated earlier, Py-1 to Py-5 precipitation was associated in space and in time with pervasive regional silicification. Čadek & Malkovský (1968) already demonstrated that the silica responsible for the silicification comes from low-temperature hydrolysis of alkali feldspars (and volcanic glass) of the Teplice rhyolite body during descending groundwater circulation. The volcanic rocks themselves, however, can hardly be the source of all the observed variations in As, Ni, Co contents in the studied pyrites because: i) trace element contents in magmatic bodies on regional scale are relatively homogeneous (average contents for acidic volcanic rocks of the Altenberg–Teplice Caldera are: 10.2 ppm As (7.4–19.4 ppm), 9.3 ppm Ni (5–16 ppm) and 5 ppm Co (1–12 ppm); Ulrych et al. 2006); ii) groundwater flow tends further to homogenize the contents of trace elements leached from host-rocks into the fluid phase.

A drop in the As content in Py-6, contrasting with the increasing trend from Py-1 to Py-5, coupled with the sudden appearance of Co and Ni in Py-6 from cores of barite crystals, suggest a marked change in the fluid circulation pattern.

Cobalt and nickel can be mobilized from mafic and ultramafic rocks, from magmatic or hydrothermal Ni-Co-sulphidic mineralizations, or from organic matter. Although the first two sources can be found in the Krušné hory Mts, they are missing in the Jeníkov area. On the other hand, fluid circulation through the overlying Tertiary lignite beds is a likely explanation for high Ni, Co and also for moderate As contents in the fluids. Besides organic sulphur compounds and disseminated sulphides with variable As admixtures (0–8 at. % As; Weiss et al. 2001), the Tertiary lignite strata are rich in organic matter-bonded/adsorbed Ni and Co. Currently exploited lignites from the near by Bílina Mine average 7.1 ppm As, 29.2 ppm Ni and 9.3 ppm Co; A Catalogue (2007).

Moreover, stable isotope and fluid inclusion data (Ulrych et al. 2007) suggest the Tertiary lignite strata as the most likely source of sulphur for the barites (hosting our Py-6) and disqualify crystalline basement sulphides as a potential source.

All the above facts point to a shallow circulation of Py-6 fluids through the Tertiary sediments or along their contacts with the Teplice rhyolite, rather than a deep fluid circulation in the Teplice rhyolite itself. Such change in fluid circulation should be substantiated by regional stress rearrangement and a consequent extinction of tectonic activity on the Krušné hory Fault.

Although no detailed tectonic measurements have been performed on the Krušné hory Fault itself, kinematic analyses of parallel faults (Coubal & Adamovič 2000) point to a post-Pliocene ENE–WSW compression followed by an ENE–WSW extension effective until the mid-Pleistocene (Mindel, ~0.4 Ma). In contrast, no faulting younger than this age has been reported, and fluvial terraces of Riss or Würm ages in the Eger Graben show no abnormities in their vertical profiles. The data from the Eger Graben are in agreement with the data on the present tectonic stresses obtained from hydraulic fracturing and borehole breakouts (World Stress Map Project, Zoback 1992), indicating a uniform NW–SE compressional stress field for most of the Alpine-Carpathian foreland. However, no tectonic deformations related to this stress field have been observed in the Bohemian Massif. This suggests a mid-Pleistocene stress reversal, which inhibited the Krušné hory Fault activity and marked the end of the fault-scarp topographic up-building. Very probably, this event can be correlated with the herein described change in fluid flow pattern and the resulting change in mineral chemistry.

Conclusions

Mineral textures and trace element chemistry of pyrites can be used as a tool to decipher the history of fluid chemistry and circulation patterns. The studied locality in the Eger Graben in northwestern Bohemia reflects near-surface mineralization processes (silicification and associated sulphide formation) in a transition from deep, fault-driven fluid flow to subsequent shallow, topography-driven groundwater flow. Six types of pyrite (Py-1 to Py-6) were distinguished, Py-1 to Py-4 being closely associated with silicification, Py-5 shortly post-

dating it and Py-6 separated by a significant time gap from the silicification. The evolution of pyrite textures from framboids (neglecting rare Py-1 relics) to individual crystals (mostly cubes) suggests an oversaturation of early fluids with respect to pyrite and its rapid crystallization. The As contents in Py-3 and Py-4f correlate well with the theoretically predicted As solubility in FeS_2 at low temperatures (Reich & Becker 2006), while those in Py-5 (up to 7.9 wt. % As) probably correspond to metastable arsenic solid solution in pyrite.

Two different fluid circulation patterns, separated in time, can be interpreted from the trace element chemistry of pyrites: i) a progressively deepening circulation pattern of low-temperature geothermal fluids derived from the acidic volcanics in the Eger Graben basement and driven by the Krušné hory Fault propagation, and ii) shallow geothermal/groundwater circulation in contact with the Tertiary lignite beds, driven by fault-scarp topography. The former contributed to the chemistry of Py-1 to Py-5, the latter to Py-6 and barite precipitation.

Acknowledgments: This research was supported by the Grant Agency of the AS CR, Project A3013302 to JA and JZ and by the Ministry of Education Grant MSM0021620855 (JZ) and the Research Plan AV0 Z30130516 of the Academy of Sciences CR (JA). The authors wish to thank the Keramost a.s. Company for providing access to the Jeníkov Quarry. We also thank B. Kříbek and Z. Sawlowicz for their critical reviews and helpful comments.

References

A catalogue of lignite, 2007: *Severočeské doly a.s. Chomutov*, 1–19.

Abraitis P.K., Pattrick R.A.D. & Vaughan D.J. 2004: Variations in the compositional, textural and electrical properties of natural pyrite: a review. *Int. J. Min. Process.* 74, 41–59.

Aiuppa A., Avino R., Brusca L., Caliro S., Chiodini G., D'Alessandro W., Favara R., Federico C., Ginevra W., Inguaggiato S., Longo M., Pecoraino G. & Valenza M. 2006: Mineral control of arsenic content in thermal waters from volcano-hosted hydrothermal systems: Insights from island of Ischia and Phlegrean Fields (Campanian Volcanic Province, Italy). *Chem. Geol.* 229, 313–330.

Breiter K. 1997: The Teplice rhyolite (Krušné hory Mts., Czech Republic) — chemical evidence of a multiply exhausted stratified magma chamber. *Bull. Czech Geol. Surv.* 72, 205–213.

Butler I.B. & Rickard D. 2000: Framboidal pyrite formation via the oxidation of iron (II) monosulfide by hydrogen sulphide. *Geochim. Cosmochim. Acta* 64, 2665–2672.

Cajz V. 2000: Proposal of lithostratigraphy for the České středohoří Mts. volcanics. *Bull. Czech Geol. Surv.* 75, 7–16.

Cleverley J.S., Benning L.G. & Mountain B.W. 2003: Reaction path modelling in the As-S system: a case study for geothermal As transport. *Appl. Geochemistry* 18, 1325–1345.

Coubal M. & Adamovič J. 2000: Youngest tectonic activity on faults in the SW part of the Most Basin. *Geolines* 10, 15–17.

Čadek J. & Malkovský M. 1968: Silicification of Upper Cretaceous rocks in the Teplice area. *Sbor. Geol. Věd, Geol.* 14, 71–87 (in Czech).

Čadek J., Kačura G. & Malkovský M. 1963: Genetic relationships between thermal waters and neoidic mineralization of rocks in the area of Teplice and Ústí nad Labem. *Věst. Ústř. Úst. Geol.* 38, 265–268 (in Czech).

Čadek J., Kačura G. & Malkovský M. 1964: Fluorite occurrences in the area of Teplice Spa in Bohemia and their genesis. *Sbor. Geol. Věd, Ložisk. Geol.* 3, 7–41 (in Czech).

Čadek J., Hazdrová M., Kačura G., Krásný J. & Malkovský M. 1968: Hydrogeology of thermal waters in the area of Teplice and Ústí nad Labem. *Sbor. Geol. Věd, HIG* 6, 7–207 (in Czech).

Čech S. & Váně M. 1988: Problems of the development of Cenomanian and Lower Turonian rocks in the Krušné hory Mts. piedmont region. *Čas. Mineral. Geol.* 33, 395–410 (in Czech).

Fengl M. 1995: Jílové-Sněžník fluorite deposit near Děčín. In: Breiter K. & Seltmann R. (Eds.): Ore mineralizations of the Krušné hory Mts. (Erzgebirge). Excursion guide. *Third Biennal SGA Meeting, August 28–31, 1995, Prague*, 113–118.

Fournier R.O. & Potter II, R.W. 1982: A revised and expanded silica (quartz) geothermometer. *Geothermal Resources Council Bulletin,* November, 3–12.

Fournier R.O. & Truesdell A.H. 1973: An empirical Na–K–Ca geothermometer for natural waters. *Geochim. Cosmochim. Acta* 43, 1543–1550.

Hladíková J., Čadek J., Šmejkal V. & Vavřín V. 1979: Isotopic study of oxygen and carbon in carbonates of the Bohemian Cretaceous Basin. *Sbor. Geol. Věd, LG* 20, 37–48.

Höhndorf A., Kämpf H. & Dulski P. 1994: Sm/Nd and Rb/Sr isotopic investigations on fluorite mineralization of the eastern Erzgebirge. In: Seltmann R., Kämpf H. & Möller P. (Eds.): Metallogeny of collisional orogens. *Czech Geol. Surv.*, Praha, 116–128.

Kharaka Y.K. & Mariner R.H. 1989: Chemical geothermometers and their application to formation waters from sedimentary basins. In: Naeser N.D. & McCollon R.H. (Eds.): Thermal history of sedimentary basins. *Springer, New York*, 99–117.

Klemm D. 1965: Synthesen und Analysen in den Dreiecksdiagrammen FeAsS-CoAsS-NiAsS und FeS2-CoS2-NiS2. *Neu. Jb. Miner., Abh.* 103, 205–255.

Langmuir D. 1996: Aqueous environmental geochemistry. *Prentice Hall*, 1–600.

Lefticariu L., Pratt L.M. & Ripley E.M. 2006: Mineralogic and sulfur isotopic effects accompanying oxidation of pyrite in millimolar solutions of hydrogen peroxide at temperatures from 4 to 150 °C. *Geochim. Cosmochim. Acta* 70, 19, 4889–4905.

Malkovský M. 1980: Model of the origin of the Tertiary basins at the foot of the Krušné hory Mts.: volcano-tectonic subsidence. *Věst. Ústř. Úst. Geol.* 55, 141–150.

Ohfuji H. & Rickard D. 2005: Experimental syntheses of framboids — a review. *Earth Sci. Rev.* 71, 147–170.

Parkhurst D.L. & Appelo C.A.J. 1999: User's guide to PhreeqC (version 2) — a computer program for speciation, batch-reaction, one-dimensional transport, and inverse geochemical calculations. *USGS Water-Resources Investigations Report,* Denver, Colorado, 99–4259, 1–326.

Reich M. & Becker U. 2006: First-principles calculations of the thermodynamic mixing properties of arsenic incorporation into pyrite and marcasite. *Chem. Geol.* 225, 278–290.

Revil A. & Cathles L.M. 2002: Fluid transport by solitary waves along growing faults — A field example from the South Eugene Island Basin, Gulf of Mexico. *Earth Planet. Sci. Lett.* 202, 321–335.

Sibson R.H., Moore J.Mc.M. & Rankin A.H. 1975: Seismic pumping — a hydrothermal fluid transport mechanism. *J. Geol. Soc. London* 131, 653–659.

Ulrych J., Pešek J., Štěpánková-Svobodová J., Bosák P., Lloyd

F.E., von Seckendorff V., Lang M. & Novák J.K. 2006: Permo-Carboniferous volcanism in late Variscan continental basins of the Bohemian Massif (Czech Republic): geochemical characteristic. *Chem. Erde, Geochemistry* 66, 37–56.

Ulrych J., Adamovič J., Žák K., Frána J., Řanda Z., Langrová A., Skála R. & Chvátal M. 2007: Cenozoic "radiobarite" occurrences in the Ohře (Eger) Rift, Bohemian Massif: Mineralogical and geochemical revision. *Chem. Erde, Geochemistry* 67, 301–312.

Váně M. 1961: A contribution to the lithostratigraphical position of quartzites at Salesiova výšina Hill, North Bohemian Brown Coal Basin. *Čas. Mineral. Geol.* 6, 346–355 (in Czech).

Wilkin R.T., Barnes H.L. & Brantley S.L. 1996: The size distribution of framboidal pyrite in modern sediments: An indicator of redox conditions. *Geochim. Cosmochim. Acta* 60, 3897–3912.

Williamson M.A. & Rimstidt J.D. 1994: The kinetics and electrochemical rate-determining step of aqueous pyrite oxidation. *Geochim. Cosmochim. Acta* 58, 5443–5454.

Zachariáš J., Adamovič J. & Konečný P., in prep: Uraninite-pyrite association, a sensitive indicator of changes in fluid chemistry: element gains and losses.

Zoback M.L. 1992: First and second order patterns of stress in the lithosphere: the World Stress Map project. *J. Geophys. Res.* 97, 11703–11728.